Feasibility assessment of parallelized helical drilling

David Brinkmeier,[a,b,*] **Volkher Onuseit**,[a] **and Thomas Graf**[a]
[a]University of Stuttgart, Institut für Strahlwerkzeuge, Stuttgart, Germany
[b]University of Stuttgart, Graduate School of Advanced Manufacturing Engineering, Stuttgart, Germany

Abstract. With the average power of commercial ultrafast lasers reaching the kW-level, process parallelization is required to avoid detrimental quality issues, such as caused by heat accumulation. This is especially relevant in the case of helical drilling, as the processing strategy is only employed when precise geometry, high-quality surface finish, tight tolerances, and high reproducibility are a priority. We illustrate that parallelization by means of a multipass process is conceptually attractive for pulsed drilling processes, but also challenging due to limitations imposed by the properties of appropriate beam-steering devices. While paraxial beam propagation methods applied to the suggested setup predict no aberrations, deviations from the idealized solution are a concern. Our experimental proof-of-principle investigations show that parallelization by means of a deflector preceding the helical drilling optics is possible while ensuring nearly identical processing parameters for all parallelly processed boreholes. [DOI: 10.1117/1.OE.62.3.035106]

Keywords: laser material processing; helical drilling; helical drilling optics; laser beam delivery.

Paper 20221442G received Dec. 14, 2022; accepted for publication Mar. 7, 2023; published online Mar. 29, 2023.

1 Introduction

With the advent of kW-class ultrafast lasers,[1–7] heat accumulation effects[8,9] that occur during machining require parallelization techniques to increase productivity, while maintaining processing quality. Of the various laser-based drilling processes,[10] helical drilling is the variant which is employed when the borehole shape, surface finish, and reproducibility are paramount. With helical drilling the hole geometry, shape, and orientation is primarily determined by the path and the inclination of the laser beam[10] relative to the work piece.

In the case of circular drillings, helical drilling optics are commonly applied, which often offer independent adjustment of the diameter of the helical beam path and the angle of incidence of the beam on the work piece. The helical drilling system usually consists of a rotational unit, henceforth referred to as helical drilling optics, and a focusing lens. More generally, any optical system, which can produce a rotating tilt and a rotating lateral offset at its output, can be considered a helical drilling optics. Given the high costs of the currently available helical drilling systems,[11–14] it is not attractive to implement parallelization approaches in which several of these systems are applied in parallel.

We therefore suggest combining a scanning system with one single helical drilling optics, with emphasis on the fact that the scan system shall precede the helical drilling optics. Such a configuration allows for the use of fast optical elements whose free (active) beam aperture is limited and/or of those whose acceptance angles are limited. Both considerations apply to acousto-optic modulators and deflectors, which are the only commercially available types of beam-steering device that offers the unique combination[15–17] of

1. μrad-level positioning accuracy, as is required when repeatedly targeting the borehole inlet of a precision microhole in a multipass process.

*Address all correspondence to David Brinkmeier, david.brinkmeier@ifsw.uni-stuttgart.de

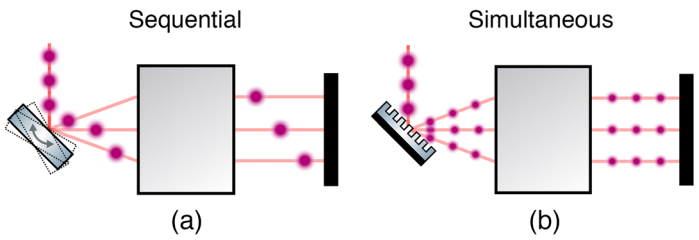

Fig. 1 Principles of parallelization in pulsed laser processing: (a) Sequential processing through fast scanning and (b) simultaneous processing through beam-splitting.

2. Response times that are capable of spatially demultiplexing pulses which are delivered at repetition rates of <MHz, while simultaneously offering active apertures that are large enough to withstand the energy densities that are provided by kW-class ultrafast lasers [It is worth noting that the response time and the size of the active aperture are conflicting objectives in the design of an acousto-optical device, where an important limiting factor is the material-specific acoustic velocity. By balancing the response time against the energy density (by means of decreasing/increasing the size of the active aperture, respectively) one finds that many kW-class ultrafast lasers already exceed the theoretical limits of these devices, exacerbating the lack of suitable alternatives.].

When synchronized with the processing laser, the combination of the helical drilling optics with a fast beam deflector allows for a sequential parallelization of the machining process in which the consecutive pulses are distributed sequentially to a number of holes drilled in parallel, as shown in Fig. 1(a). Such a strategy results in a reduction of the pulse repetition rate per borehole, while still exploiting the full available pulse energy (required to produce deep holes[18]) and the available average laser power.

A reduction of the pulse repetition rate incident on the individual holes, and the consequently increased spatial separation of the pulses within each hole, reduces heat accumulation effects[8,9] and particle shielding,[19–22] which is pronounced in drilling processes[21,23] and has no impact on the achievable depth of the borehole.[24]

In contrast, simultaneous parallelization by conventional beam-splitting,[25] as shown in Fig. 1(b), leads to a reduction of the achievable depth by reducing the peak fluence impinging on the individual boreholes, and only has a minor impact on particle shielding effects, which depend primarily on the pulse repetition rate.[21,23,26,27] While both strategies (sequential and simultaneous parallelization) have merit and in fact may be applied at the same time, a feasible solution to the former is of major interest, because it is better suited to the process and harder to achieve due to the constraints imposed by compatible beam-steering devices.

The combination of a helical drilling optics with an additional beam deflector must offer a scan field within which deviations from the intended helical drilling parameters and beam parameters, are negligible. Deviations of the machining parameters throughout the scan field result in variations of the geometries of adjacent boreholes, which are regarded to be unacceptable for helical drilling processes.

The aim here is to provide the experimental validation of the optical configuration to prove that these goals can be met in practice. For the validation and measurements, a low-power laser and a galvanometer scanner were used to show that virtually identical properties of the processing beam and its circular paths can be obtained throughout the working area. The theoretical considerations that lead to the presented setup and to the choice of the specific type as well as the implementation of the used helical drilling optics will be addressed in a separate work concerned with the fundamental properties of helical drilling optics as they pertain to the parallelization of the helical drilling process.

2 Motivation and Setup

Heat accumulated during the drilling process leads to thermal damage in the remaining adjacent material after the process and leads to increased surface roughness[28] as well as burrs[27–29]

surrounding the inlet of the borehole. The formation of burrs, molten material on the wall of the borehole, and the ejection of liquid droplets also occurs at low pulse repetition rates and low average powers when the applied fluence is high;[30] however, high fluences are a necessity for ultra-short pulsed laser drilling since the achievable depth of high-quality boreholes with a given diameter of the opening is limited by the available pulse energy.[18,24,31,32] The heat accumulation that leads to significant quality issues by additional generation of excessive melt increases with increasing pulse energies E_p and increasing pulse repetition rate f_{rep}.[8,9] The upper limit $f_{\mathrm{rep,crit}}$ of the repetition rate imposed by heat accumulation and its dependence on the pulse energy was discussed and verified by more than 1000 percussion-drilling experiments[33] and leads to the conclusion that the detrimental influence of heat accumulation can only be avoided by corresponding parallelization approaches. The findings likewise also apply to helical drilling with the difference that parallelization is even more difficult to implement here.

Additional detrimental effects that are aggravated by an increased pulse repetition rate are related to the laser-atmosphere interaction. It has been shown that the remaining cloud of ablation products after each laser pulse consists of charged particles[34–36] capable of affecting the absorption of subsequent pulses for up to several milliseconds. The interaction is characterized by increased scattering and absorption[20,37–40] of the irradiated radiation prior to reaching the surface of the borehole as the radiation passes the hot and weakly ionized gas in the blind hole. The result is an increased radiative, conductive, and convective heat exchange between plasma and substrate[41,42] as subsequent pulses are applied. This mechanism has previously been referred to as a secondary drilling tool[19,43] and results in thermal effects and material removal rates exceeding the expectations of isolated thermal modeling[29] at the cost of processing quality.

Hence, a strong argument can be made for a sequential parallelization of drilling with ultrafast lasers, in which the available laser power $P_{\mathrm{avg}} = E_p \cdot f_{\mathrm{rep}}$ is distributed to n boreholes.

In such a method, the beam is displaced between n boreholes for successive pulses. A new borehole is targeted after every timespan $1/f_{\mathrm{rep}}$, and each borehole is hit by a laser pulse in intervals of n/f_{rep}. When the pulse repetition rate per borehole is lowered to $f_{\mathrm{rep}}/n \leq f_{\mathrm{rep,crit}}$ by a suitable choice of n, the larger temporal and spatial separation of the incident pulses in the hole resolves heat accumulation effects without (the need for) a reduction of the pulse energy E_p incident on the individual boreholes. In contrast, when avoiding heat accumulation through the approach of simultaneous parallelization by beam-splitting, depending on the pulse repetition rate f_{rep} of the laser, the pulse energy $E_p/n \leq E_{p,\mathrm{crit}}$ that is applicable at most to avoid heat accumulation may even be so low that a drilling process is not possible or cannot reach the desired depth.[33]

Of course, in practice, n is also constrained by the finite dimensions of the workpiece and/or the limited scan field provided by the optical system, which in turn limits the maximum average laser power that can be used.

For helical drilling, the sequential parallelization strategy can be implemented using a fast and accurate beam deflector in conjunction with a conventional helical drilling optics as outlined in the following.

For the optical characterization of such a setup, the helical drilling optics that was chosen for the measurements is composed of rotating wedge plates and provides independent adjustment of the helical drilling diameter and the angle of incidence (trepanning angle) through a relative axial and rotational movement of the wedge plates. More details on the specific setup are given in Refs. 44–47. A beam deflector was placed in the path before the helical drilling optics to repeatedly relocate the position of the helical drilling process on the workpiece without having to move the helical drilling optics or workpiece and which must be accomplished without affecting the parameter of helical drilling or the beam. In addition, it was specified that adjacent boreholes must not be tilted with respect to each other or experience deviating drilling parameters.

By principle any of the common deflection systems, e.g., mechanical, electro-optical, or acousto-optical devices, or combinations thereof are suitable for the proposed parallelization approach. The implemented experimental setup used for the proof of principle in the framework of this study is schematically shown in Fig. 2.

The relay lenses (2,3) image the exit pupil of the beam deflector (1) onto the entrance pupil of the telecentric focusing lens (6), ensuring a telecentric scanning operation of the beam deflector in all planes after the focusing lens (6) when the imaging condition is satisfied over the parameter

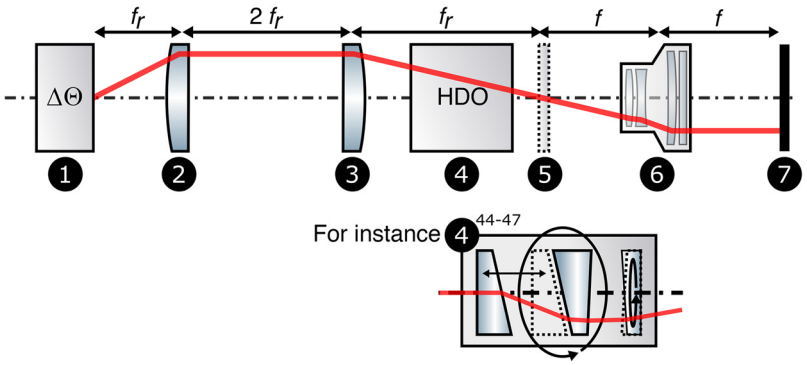

Fig. 2 Principal setup, from left to right: (1) scan system for beam deflection, (2) and (3) relay lens with focal length f_r, (4) helical drilling optics, (5) image plane of (1) and (6) Fourier plane of telecentric *f*-theta focusing optics with focal length f and position for placement of an additional scan system or beam splitter, and (7) work piece = location of measurement system in this study.

range provided by the beam deflector as well as the parameter range of the helical drilling optics (4). With this arrangement, a deflection by the angle θ induced by the deflector (1) leads to a displacement of the drilling position by $\approx f\theta$ in the focal plane on the surface of the workpiece (7).

Paraxial optics suggest that the subsystem (1,2,3,6) and the subsystem (4,6) operate independently, the systems are however at least weakly coupled, which is why deviations in the aforementioned condition are expected. Indeed, the motivation for this work is to answer the question whether the deviations are substantial enough to negatively affect the properties of the laser beam at the location of the many laterally displaced spots in the working area, i.e., whether or not such a parallelized helical drilling system meets the requirements necessary to be of practical interest. For the characterization of the optical system, the work piece (7) was replaced with a camera system, as outlined in the following section. This was done for two reasons: First, it allows to measure the performance of the superposition of the deflection systems isolated from secondary effects that could occur in the ablation process (e.g., effects related to high power densities traversing the ambient atmosphere, optical components, as well as the laser-matter interaction itself), and second, it allows to confirm the proof of principle without requiring an (experimental) fast deflection unit.

For convenience, the image/Fourier plane (5) was positioned immediately after and outside the helical drilling optics, making it accessible for measurement and adjustment purposes and avoiding the need for placement of optical elements inside the rotating unit.

The effective working area at (7) was limited to a circular scan field by the condition $\theta < 24$ mrad given by the optical path length of the used helical drilling optic (4) and the apertures of its optical elements.

The scan area is further reduced to $\theta < 18$ mrad when the diameter of the input beam is considered in the available setup, when using Siegman's 99% criterion.[48] A helical drilling optics specifically designed to be used in this way could yield a larger scan area, but the scan area of the present setup is large enough to investigate the feasibility of a meaningful process parallelization of helical drilling. With the present setup the working area had a diameter of 4.5 mm. The optical relay (2 and 3) was implemented using two plano-convex lenses, which is diffraction-limited according to numerical analysis for the used beam diameter and scan angles θ. A Scanlab intelliSCAN 20 galvanometer scanner was chosen as the beam deflector. The setup was adjusted such that one of the galvanometer mirrors is reimaged in plane (5). A photograph of the setup used for the measurements is shown in Fig. 3.

3 Measurement Methodology and Definitions

Apart from the properties of the deployed laser, polarization state, and processed material, the helical drilling process is fully defined by the scan path at the position of the workpiece and the

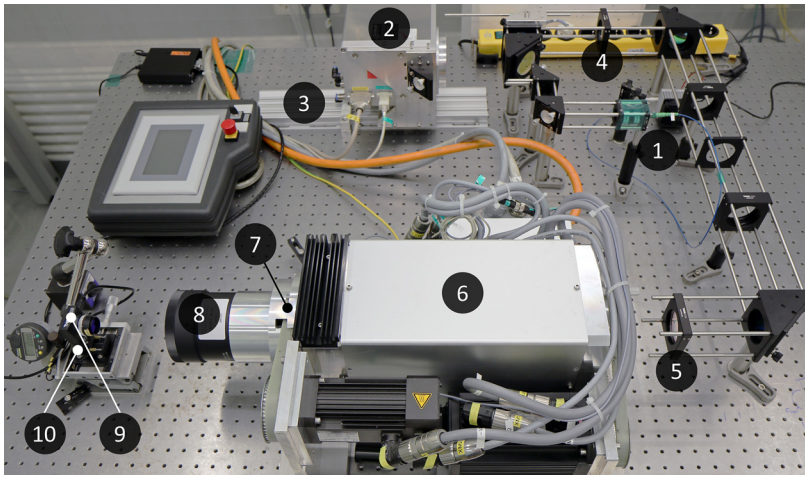

Fig. 3 Experimental setup: (1) single-mode fiber laser (Integrated Optics 1030L-25B), (2) galvanic two-mirror scanner (Scanlab intelliScan 20 (XY-100 protocol)), (3) dovetail with micrometer screw for axial adjustment of the scanner with respect to the object plane of the relay optics, (4,5) relay optics (with Edmund Optics 67-589 lenses), (6) helical drilling optics, (7) position of back focal plane of (8) focusing lens (Sill S4LFT4127-328), (9) camera for diagnostics of the beam steering (IDS UI154xLE-M with 5.2-μm pixel pitch), and (10) piezo stage (Linos MS-30 XY). The lens (8) is mounted to (6), but does not rotate.

beam parameters. For helical drilling, these parameters are the drilling axis, the trepan angle, the trepan radius measured in the focal plane, the beam diameter in the focal plane, and the divergence of the beam. For a successful parallelization of the helical drilling process, the beam incident to the adjacent boreholes that are drilled in parallel within the working area must yield identical properties and identical orientation with respect to the processed surface. Thus, all processing parameters shall be identical, except for the laterally shifted positions of the drilling axes on the workpiece. The definitions and the corresponding measurement approach are shown schematically in Fig. 4. The time-averaged distribution of the irradiance produced by the beam that is moved on a circular path by the trepanning optics is recorded by means of a camera in three different planes which are perpendicular to the of the beam entering the trepanning optics leads to a superimposed displacement of the generated irradiance distributions by the same distance $f \cdot \theta$ in all the three planes I, II, and III. Plane I coincides with the focal plane and is thought to lie on the surface of a drilled workpiece; plane II shall represent the middle of the workpiece; and plane III its rear surface. The evolution of the irradiance distributions over the three planes, as obtained with a deflection of $\theta = 0$, are highlighted in blue and serve as a reference.

The position and orientation of the drilling axes (dashed lines) are extracted from the measurement by a least-squares orthogonal distance regression line through the centers of the measured distributions of the irradiance.

To achieve identical drilling results everywhere in the working area, the drilling axes should all be parallel to the drilling axis obtained with the reference deflection $(\theta = 0)$. The parallelism error α_{err} is defined as the tilt angle between the drilling axis obtained with a deflection $(\theta \neq 0)$ and the axis of the reference with $(\theta = 0)$. The error α_{err} is similar to the telecentricity error[49] in a telecentric scan system, which describes the non-parallelism of rays exiting toward the work piece. In our arrangement, α_{err} is defined as the deviation of the helical drilling axis and is of concern even at small values because it affects the lateral spacing between adjacent boreholes, resulting in a distorted drilling pattern. The parallelism error α_{err} is calculated as the absolute angle between the direction vector obtained for $(\theta \neq 0)$ and direction vector obtained for $(\theta = 0)$.

With $\alpha_{\mathrm{err}} \neq 0$, the lateral separation with respect to the reference measurements is increased from $\approx f\theta$ in the focal plane I to $\approx f\theta + \alpha_{\mathrm{err}} z_{\mathrm{I-III}}$ in the plane III, where $z_{\mathrm{I-III}}$ is the distance between the planes I and III. Hence the parallelism error is magnified proportional to the

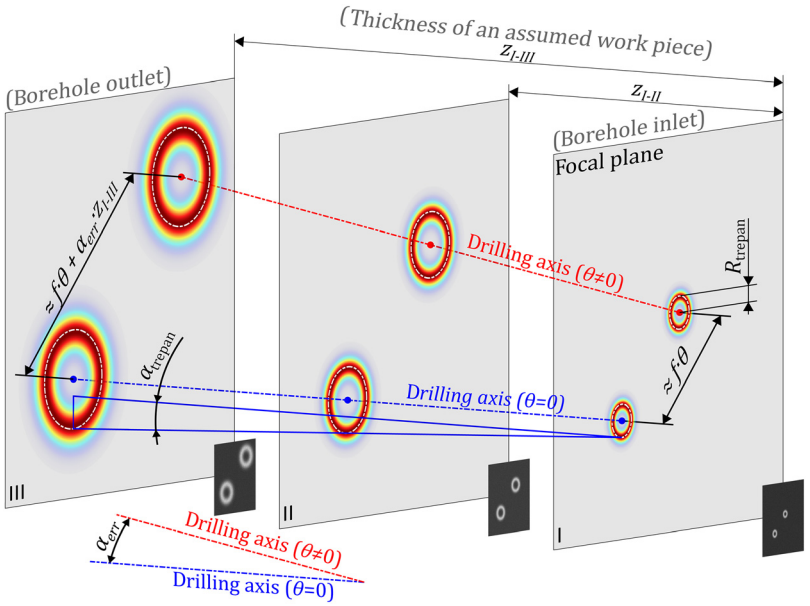

Fig. 4 Measurement approach and definitions. The time-averaged distributions of the irradiance are recorded in three planes (I, II, and III) which are perpendicular to the z axis to determine the drilling axis and characterize the evolution of the irradiance distributions.

thickness of a work piece. This consideration motivates, or rather demands, the use of a telecentric focusing system.

The trepan angle α_{trepan} is the angle between the drilling axis and the axis of the (trepanning) beam, i.e., the half angle of the cone defined by the trepanning motion. The trepan angle α_{trepan} is also extracted from the measured irradiance distributions for the present study. The trepanning radius R_{trepan} is defined as the radius of the circular beam path in the focal plane I. In any other plane the trepanning radius is implicitly defined by R_{trepan} and α_{trepan}. This simplified characterization of the beam propagation is sufficient for the intended feasibility analysis. A more detailed discussion of the working principle of the helical drilling optics [44,45,50] and the resulting 3D movements of the beam is not necessary and is beyond the scope of this paper.

For a precise and robust determination of the quantities displayed in Fig. 4, the theoretically expected distribution of the irradiance was fitted to the ones measured using the camera. This distribution is given by the time-averaged irradiance produced by a Gaussian beam that is moved on a circular path with radius R_{trepan}, as sketched in Fig. 5.

Using the cosine law $(r')^2 = R_{\text{trepan}}^2 + r^2 - 2R_{\text{trepan}} r \cdot \cos(\varphi)$ and the intensity distribution $J_0 e^{-2(\frac{r'}{w})^2}$ of a Gaussian beam, where J_0 is the peak intensity, r' the radial coordinate with its

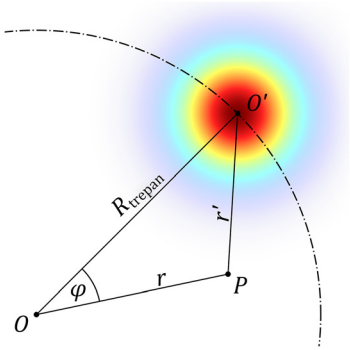

Fig. 5 A Gaussian beam with its axis located at O' traveling on a circular path (dash-dotted line) with radius R_{trepan} about the origin O. The time-averaged irradiance at (any) point P on the camera sensor (in the plane) is the superposition of irradiances for $\varphi \in [0,2\pi)$.

origin on the axis of the beam, and w is the beam radius, the time averaged irradiance $J(r)$ is given by

$$J(r) = J_0 e^{-2\left(\frac{R_{\text{trepan}}^2 + r^2}{w^2}\right)} \cdot \frac{1}{2\pi} \int_0^{2\pi} e^{\frac{4R_{\text{trepan}} r}{w^2} \cdot \cos(\varphi)} \mathrm{d}\varphi, \tag{1}$$

where $r = 0$ is the center of the circular path. Here it is implicitly assumed that the trepanning angle is so small that $\cos(\alpha_{\text{trepan}}) \approx 1$ and hence the distribution of the irradiance on the workpiece can very accurately be approximated by the unstretched intensity distribution of the beam. The integral in Eq. (1) corresponds to the modified Bessel function of the first kind of order zero I_0 (cf. Ref. 51, Eq. 9.6.16, p. 376), hence

$$\frac{1}{2\pi} \int_0^{2\pi} e^{\frac{4R_{\text{trepan}} r}{w^2} \cdot \cos(\varphi)} \mathrm{d}\varphi = \frac{1}{\pi} \int_0^{\pi} e^{\frac{4R_{\text{trepan}} r}{w^2} \cdot \cos(\varphi)} \mathrm{d}\varphi = \mathrm{I}_0\left(\frac{4R_{\text{trepan}} r}{w^2}\right). \tag{2}$$

To determine the quantities shown in Fig. 4 from the measured irradiances, the distribution

$$J(r) = J_0 \cdot e^{-2\left(\frac{R_{\text{trepan}}^2 + r^2}{w^2}\right)} \cdot \mathrm{I}_0\left(\frac{4R_{\text{trepan}} r}{w^2}\right) + c, \tag{3}$$

was fitted to the time-averaged distributions of the irradiance measured by the CCD camera sensor, where c was introduced to account for a constant gray level offset throughout the image. Equation (3) is in good agreement with the measured irradiance profiles, as shown in Fig. 6.

4 Results

To assess by what amount the local drilling parameters are affected when the processing position is scanned across the working area, see Fig. 4, the resulting distributions of the time-averaged irradiance and their evolution along the propagation in z-direction was measured for different scan angles θ ranging from -15 to 15 mrad in steps of 5 mrad.

The measurement performed with $\theta = 0$ mrad serves as a reference. The measurements were conducted for two settings of the helical drilling optics, specifically one close to the minimum achievable values with radius $R_{\text{trepan}} = 40.6\ \mu\text{m}$ and the angle $\alpha_{\text{trepan}} = 0.26$ deg and one where the two parameters were set to practically the maximum possible values ($R_{\text{trepan}} = 313.3\ \mu\text{m}$,

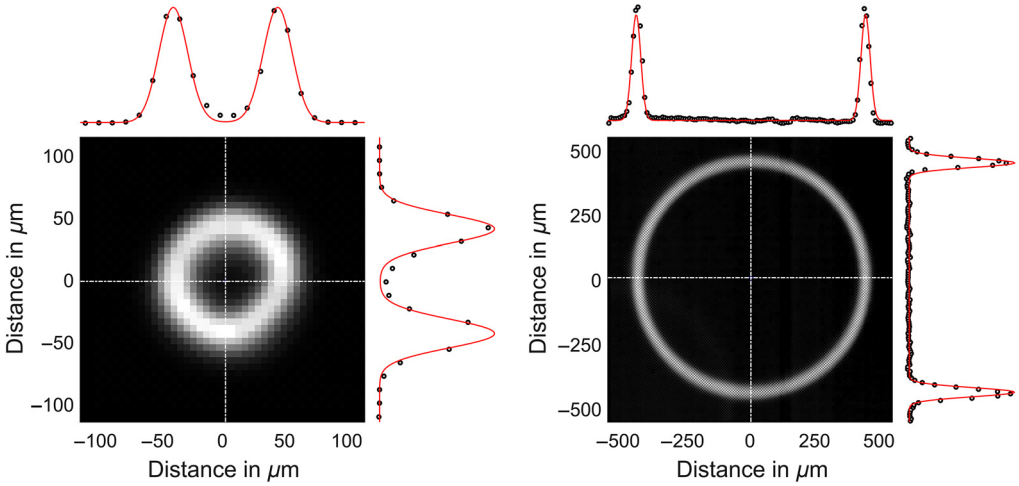

Fig. 6 Comparison of fit (red curves) and measured profiles (dots) of cross sections (along the white lines) through the irradiance distributions (pictures) recorded by the camera for two different helical drilling parameters.

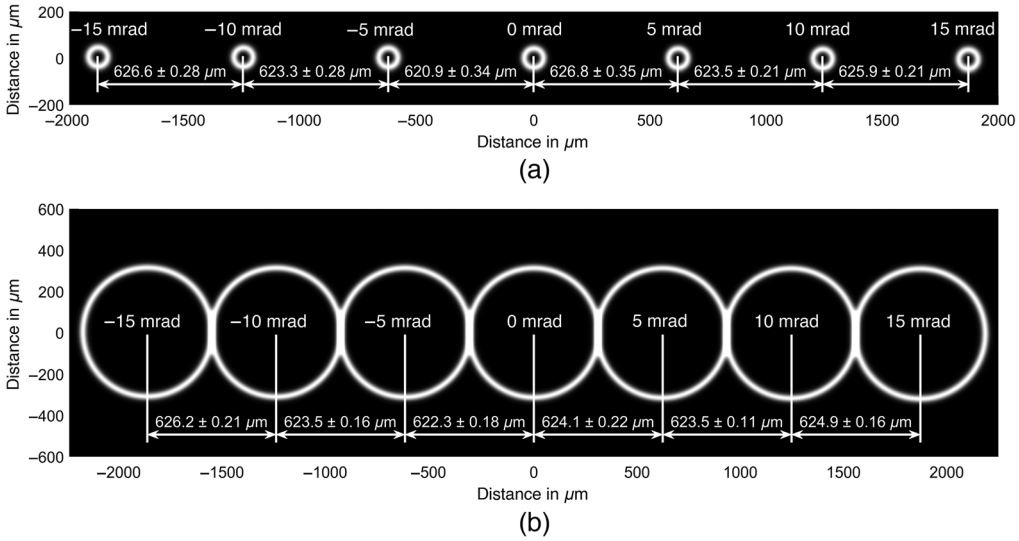

Fig. 7 Distance between the centroids of the time-averaged irradiance measured in the focal plane at adjacent measurement locations. The given uncertainties correspond to one standard deviation in radial direction about the centroids, 50 measurements for each value of the scan angle Θ were recorded. (a) Trepanning radius $R_{\text{trepan}} = 40.6\ \mu\text{m}$ and trepanning angle $\alpha_{\text{trepan}} = 0.26$ deg. (b) $R_{\text{trepan}} = 313.3\ \mu\text{m}$ and trepanning angle $\alpha_{\text{trepan}} = 4.37$ deg.

$\alpha_{\text{trepan}} = 4.37$ deg). One may assume that all other possible helical drilling parameters yield aberrations with values in between these two extremes.

The focal length of the used telecentric f-Θ lens is 125.4 mm $\pm$ 1.5% according to the manufacturer's specification. The expected lateral displacement of the adjacent irradiance distributions therefore amounts to 5 mrad $\cdot$ 125.4 mm $= 627\ \mu$m. This is consistent with the measured values shown in Fig. 7 when one takes into account the angular resolution of the galvanometer scanner, its positioning repeatability, and the tolerance of the focal length of the focusing optics. The pointing deviation of the drilling axis is limited to about 10 μrad, as indicated by the results presented in Fig. 7, where less than one micrometer deviation of the drilling axis in the focal plane, throughout the trepanning motion, was recorded.

The measurements of the parameters which govern the helical drilling process (see Fig. 4) for the first setting of the helical drilling optics are provided in Fig. 8. The radius of the laser beam measured in the plane $i \in \{\text{I}, \text{II}, \text{III}\}$ obtained with the scan angle θ is denoted by $w_i(\theta)$. The trepanning beam was recorded at a camera framerate of 50 fps for a total of 15,000 frames and the helical drilling optics was set to 50 revolutions per minute. The image data were post-processed by averaging 300 frames, corresponding to the next smallest integer of (6) full revolutions of the trepanning beam. The slow rotational frequency was chosen to minimize the effects of vibrations transmitted from the helical drilling optics to the optical table and measurement setup. For each measurement (scan angle θ and plane I through III), a total of 50 parameter sets were thus obtained by fitting Eq. (3) to the data. The given uncertainties correspond to one standard deviation of measurement accuracy throughout these 50 results per measurement.

The results in Fig. 8(a) show that the trepanning angle α_{trepan} remains virtually unaffected over the scan range. Assuming, e.g., a 5-mm-thick work piece, a 0.01 deg deviation for the trepanning angle translates into a <1 μm deviation of the trepanning radius in plane III (0.01 deg $\cdot\ 180/\pi \cdot$ 5 mm $= 0.87\ \mu$m), cf. Fig. 4.

While permitted deviations α_{err} of the individual drilling axes can only be defined for a specific application given its requirements, a value of <0.1 deg may be considered as a small error. The maximum measured deviation $\alpha_{\text{err}}(15\ \text{mrad}) \approx 0.08$ deg (tilt) of the drilling axis at the maximum scan angle, e.g., would translate to a lateral runout of 7 μm between entrance- and exit of an assumed hole in a 5-mm-thick work piece ($\alpha_{\text{err}} \cdot z_{\text{I–III}} = 0.08$ deg $\cdot\ 180/\pi \cdot$ 5 mm $= 7\ \mu$m, cf. Fig. 4), when assuming that the center of the resulting borehole coincides with the center of the time-averaged intensity distribution. The smallest achievable error α_{err}

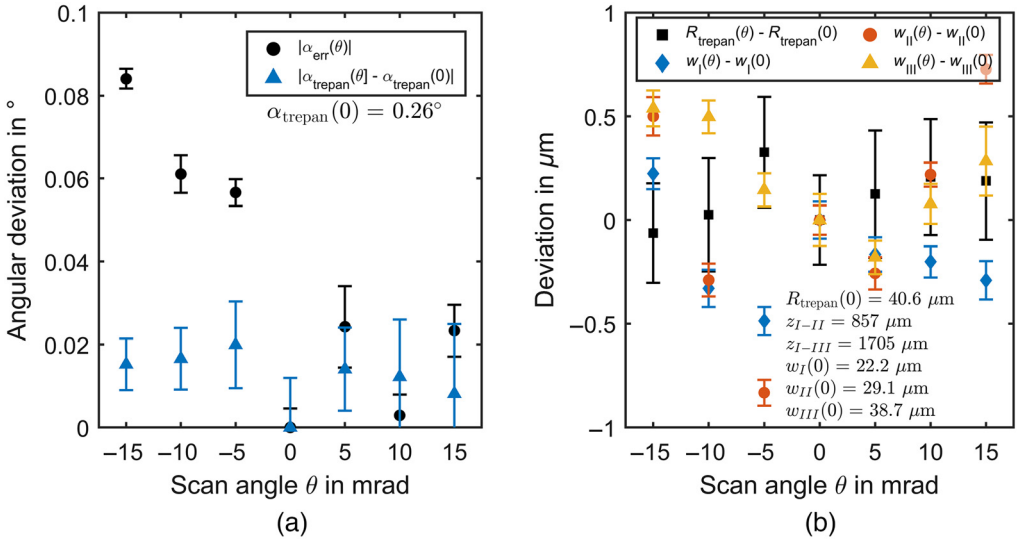

Fig. 8 Parallelism error $\alpha_{\mathrm{err}}(\theta)$ and deviation $\Delta\alpha_{\mathrm{trepan}}\theta = \alpha_{\mathrm{trepan}}(\theta) - \alpha_{\mathrm{trepan}}(0)$ of the trepanning angle (a) as well as the deviations of the trepan radius $\Delta R_{\mathrm{trepan}}\theta = R_{\mathrm{trepan}}(\theta) - R_{\mathrm{trepan}}(0)$ and beam radius $\Delta w\theta = \Delta w\theta - w(0)$ in each of the measurement planes I through III (b) measured as a function of the scan angle θ with respect to the values obtained with $\theta = 0$. $R_{\mathrm{trepan}}0 = 40.6$ μm and $\alpha_{\mathrm{trepan}}0 = 0.26$ deg.

corresponds to the telecentricity error of the f-Θ lens in a single-mirror scan setup where the scan mirror is positioned at the ideal distance from the lens. This error was calculated numerically to be 0.0314 deg at a scan angle of 15 mrad, confirming the almost ideal performance of the experimentally tested setup.

The results in Fig. 9(a) show that the radii of the laser beam and the trepanning paths only exhibit submicron deviations from the reference values throughout the scan-field and the measurement planes. Compared to the reference values at $\theta = 0$ mrad the maximum relative deviations correspond to $(-2.2 \pm 0.31)\%$ for 0 w_{I}, $(-2.86 \pm 0.22)\%$ for w_{II}, $(3.6 \pm 0.43)\%$ for w_{III}, and $(0.94 \pm 0.69)\%$ for R_{trepan}.

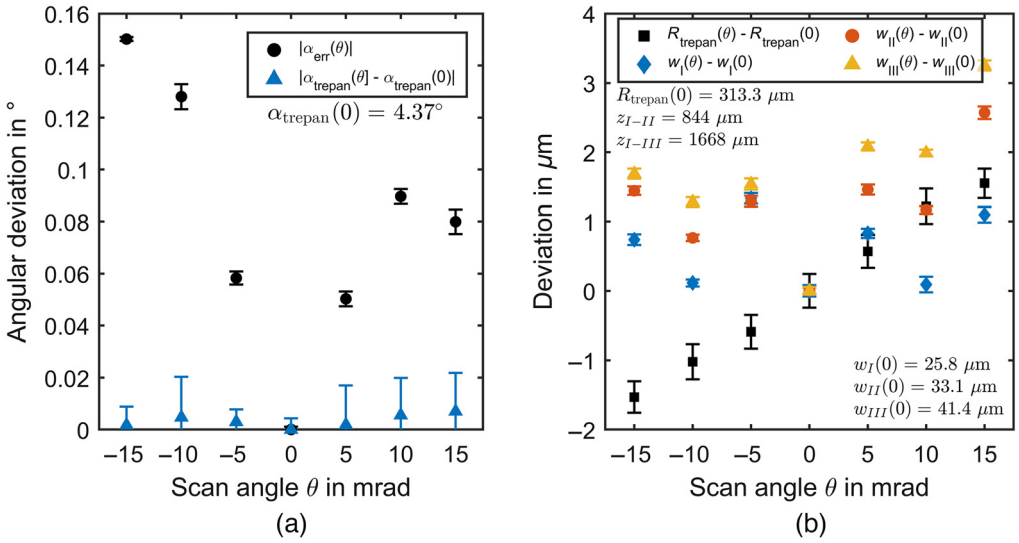

Fig. 9 Angular deviations in degrees (a) and spatial deviations in microns (b) for the helical drilling optics operated with the maximum achievable values of drilling diameter and trepanning angle, as shown in Fig. 7(b).

Without readjustment of the optical system, the measurements were repeated with the second set of parameters for the helical drilling optics. The results are presented in Fig. 9. The measurement methodology was identical to the one described above in relation to Fig. 8.

The results presented in Fig. 9 show that, compared to the results presented in Fig. 8, the maximum deviation α_{err} of the helical drilling axis is increased roughly by a factor of two for the same scan angle θ, when the helical drilling optics is operated with the maximum values of R_{trepan} and the angle α_{trepan}. The deviation of the trepanning radius $R_{\mathrm{trepan}}(\theta)$ from the value $R_{\mathrm{trepan}}(\theta = 0)$ shows a strong dependence on the scan angle. The results of this measurement are consistent with an error resulting from the projection of the divergent circular beam path ($R_{\mathrm{trepan}}, \alpha_{\mathrm{trepan}} > 0$) sampled on a slightly tilted camera sensor but exceed the theoretically predicted aberrations of the optical setup according to which R_{trepan} should not deviate by more than 0.055% over the entire scan field and should be identical at both edges of the scan field for a perfectly aligned optical system. Despite this, the results in Fig. 9 show that the deviations measured with the experimental setup are still well tolerable for practical applications.

The deviation of the beam radius increases when moving from plane I to III. Compared to the reference value at $\theta = 0$ mrad the maximum relative deviations amount to $(5.2 \pm 0.3)\%$ for w_{I}, $(7.76 \pm 0.27)\%$ for w_{II}, $(7.85 \pm 0.17)\%$ for w_{III}, and $(0.5 \pm 0.07)\%$ for R_{trepan}.

5 Discussion

The results show that the deviations of the helical drilling parameters, while detectable within the measurement accuracy, remain very small when superimposing an additional preceding scan system with the chosen helical drilling optics. The practical significance of this result is that aberrations of adjacent borehole geometries in a parallelized processing application are likely to be very small as well. Thus, the results confirm the feasibility of the process parallelization of the helical drilling process in a way that allows to reduce the effective pulse repetition rate per location, while still exploiting a high average power, which is particularly suitable for ultrafast laser drilling with kW-class lasers.

The challenge in converting the setup into a beam delivery system for material processing is to find a suitable technology for the upstream scanning system. Given currently existing technology, this appears to be an acousto-optic deflector for lack of a better alternative. Thus, the difficulty lies in a technical realization of the setup. To name a few challenges this includes the limited size of active apertures, energy density constraints, variations of diffraction efficiency as a function of the scan angle, air breakdown in intermediate focal planes, and synchronization of the laser and scan systems.

With respect to the helical drilling optics itself it should be noted that while the system used for the study is compatible with the concept, it is not an ideal solution. An optimized helical drilling optics can specifically be designed around the constraints imposed by the additional scan system, e.g., to realize a larger scan area and minimize aberrations when used in this way. However, these considerations are secondary to the problem of the upstream scan system, which appears to be the limiting factor.

6 Conclusion

The progress of kW-class ultrafast lasers[1–7] has outpaced the advances in beam delivery systems required to enable the industrial application of these lasers in material processing.

Beam delivery systems that address this problem are those that solve the parallelization of laser material processes. These systems[52–57] consist of multiple active scan systems (or even phase modulators) and/or passive elements (such as diffractive beam splitters/shapers) that are then superimposed to generate the desired effect, such as a parallelized scanning or drilling process,[25,52,53] or scanning with beam shaping.[54,55,57] This superposition is necessary because there is currently no single technology or element that can provide the required functionality in one package. The technical challenge is to place the active and passive components in a way that considers the limitations of each component and those of the process to obtain a feasible beam delivery system.

While the solution is ultimately similar, the requirements for successful parallelization of the helical drilling process are quite different from these examples, both in terms of the optical systems used and in terms of the process constraints.

To this end, our proof of concept confirms the viability of the proposed arrangement to sequentially parallelize the helical drilling process, i.e., reduce the pulse repetition rate per drilled hole, with negligible aberrations throughout the scan field, while also being feasible when considering available technology. This is not the case for many other helical drilling optics, either due to technical limitations, such as limited apertures, but also fundamentally because the operating principle of the helical drilling optics itself is incompatible with the concept, as will be discussed in a future publication.

Acknowledgments

This research received no specific grant from any funding agency in the public, commercial, or not-for-profit sectors. The authors have no conflicts of interest to declare. There is no financial interest to report.

References

1. A. Klenke et al., "530 W, 1.3 mJ, four-channel coherently combined femtosecond fiber chirped-pulse amplification system," *Opt. Lett.* **38**(13), 2283–2285 (2013).
2. M. Mueller et al., "3.5 kW coherently combined ultrafast fiber laser," *Opt. Lett.* **43**(24), 6037–6040 (2018).
3. J.-P. Negel et al., "Ultrafast thin-disk multipass laser amplifier delivering 1.4 kW (4.7 mJ, 1030 nm) average power converted to 820 W at 515 nm and 234 W at 343 nm," *Opt. Express* **23**(16), 21064–21077 (2015).
4. M. Mueller et al., "16 channel coherently-combined ultrafast fiber laser," in *OSA Tech. Digest (Online)*, p. AW4A.3 (2017).
5. J.-P. Negel et al., "1.1 kW average output power from a thin-disk multipass amplifier for ultrashort laser pulses," *Opt. Lett.* **38**(24), 5442–5445 (2013).
6. T. Nubbemeyer et al., "1 kW, 200 mJ picosecond thin-disk laser system," *Opt. Lett.* **42**(7), 1381–1384 (2017).
7. B. E. Schmidt et al., "Highly stable, 54 mJ Yb-InnoSlab laser platform at 0.5kW average power," *Opt. Express* **25**(15), 17549–17555 (2017).
8. R. Weber et al., "Heat accumulation during pulsed laser materials processing," *Opt. Express* **22**(9), 11312–11324 (2014).
9. R. Weber et al., "Processing constraints resulting from heat accumulation during pulsed and repetitive laser materials processing," *Opt. Express* **25**(4), 3966–3979 (2017).
10. F. Dreisow et al., *Drilling with Ultrashort Laser Pulses at High Repetition Rates*, pp. 175–200, Springer, Cham & Heidelberg (2016).
11. Steinmeyer Mechatronik GmbH, "Laser drilling head SLH200," https://www.steinmeyer-mechatronik.de/en/products/laser-drilling-head/ (accessed 26 August 2019).
12. ARGES GmbH, "KOALA," https://www.arges.de/industrial-products/koala/ (accessed 26 August 2019).
13. GFH GmbH, "GL.trepan," https://gfh-gmbh.de/en/machine-building/configuration/hardware/gl-trepan (accessed 26 August 2019).
14. Dausinger & Giesen GmbH, "Helical drilling optic," https://www.dausinger-giesen.de/micromachining/helical-drilling-optic (accessed 26 August 2019).
15. G. Römer and P. Bechtold, "Electro-optic and acousto-optic laser beam scanners," *Phys. Proc.* **56**, 29–39 (2014).
16. J. Heberle et al., "Electro-optic and acousto-optic laser beam scanners," *Proc. SPIE* **9736**, 97360L (2016).
17. P. Bechtold et al., *Beam Guidance, Focal Position Shifting and Beam Profile Shaping in Ultrashort Pulsed Laser Materials Processing*, pp. 245–281, Springer, Cham & Heidelberg (2016).

18. D. Holder et al., "Analytical model for the depth progress of percussion drilling with ultrashort laser pulses," *Appl. Phys. A* **127**(5), 1–8 (2021).
19. D. Breitling et al., "Plasma effects during ablation and drilling using pulsed solid-state lasers," *Proc. SPIE* **5121**, 24–33 (2002).
20. D. Breitling, S. Klimentov, and F. Dausinger, *Interaction with Atmosphere*, pp. 75–91, Springer, Berlin (2004).
21. J. König, S. Nolte, and A. Tünnermann, "Plasma evolution during metal ablation with ultrashort laser pulses," *Opt. Express* **13**(26), 10597–10607 (2005).
22. D. Haasler and J. Finger, "Investigation of heat accumulation effects during deep hole percussion drilling by high power ultrashort pulsed laser radiation," *J. Laser Appl.* **31**(2), 22201 (2019).
23. S. Döring et al., "Hole formation process in ultrashort pulse laser percussion drilling," *Phys. Proc.* **41**, 431–440 (2013).
24. D. J. Förster et al., "Estimation of the depth limit for percussion drilling with picosecond laser pulses," *Opt. Express* **26**(9), 11546–11552 (2018).
25. N. Kaplan et al., "High-precision laser microcutting and laser microdrilling using diffractive beam-splitting and high-precision flexible beam alignment," *Proc. SPIE* **10377**, 103770K (2017).
26. A. Ancona et al., "High speed laser drilling of metals using a high repetition rate, high average power ultrafast fiber CPA system," *Opt. Express* **16**(12), 8958–8968 (2008).
27. A. Ancona et al., "Femtosecond and picosecond laser drilling of metals at high repetition rates and average powers," *Opt. Lett.* **34**(21), 3304–3306 (2009).
28. T. V. Kononenko et al., "Influence of pulse repetition rate on percussion drilling of Ti-based alloy by picosecond laser pulses," *Opt. Lasers Eng.* **103**, 65–70 (2018).
29. J. Finger and M. Reininghaus, "Effect of pulse to pulse interactions on ultra-short pulse laser drilling of steel with repetition rates up to 10 MHz," *Opt. Express* **22**(15), 18790–18799 (2014).
30. A. Michalowski et al., "Theoretical and experimental studies of ultra-short pulsed laser drilling of steel," *Proc. SPIE* **9135**, 91350R (2014).
31. S. Lazare, J. Lopez, and F. Weisbuch, "High-aspect-ratio microdrilling in polymeric materials with intense KrF laser radiation," *Appl. Phys. A* **69**(S1), S1–S6 (1999).
32. V. N. Tokarev et al., "High-aspect-ratio microdrilling of polymers with UV laser ablation: experiment with analytical model," *Appl. Phys. A* **76**(3), 385–396 (2003).
33. D. Brinkmeier et al., "Process limits for percussion drilling of stainless steel with ultrashort laser pulses at high average powers," *Appl. Phys. A* **128**(1), 35 (2022).
34. S. M. Klimentov et al., "Ablated nano-particles residing in air: characterization, elimination, and role in pulsed microdrilling," *Proc. SPIE* **6606**, 66060H (2006).
35. S. M. Klimentov et al., "Generation of long-living charged nanoparticles at ablation in air and their role in pulsed microdrilling," *Laser Phys.* **18**(6), 774–779 (2008).
36. K. W. Kolasinski, M. C. Gupta, and L. V. Zhigilei, *Plume and Nanoparticle Formation During Laser Ablation*, pp. 594–603, Elsevier, Amsterdam, Netherlands & Oxford, UK (2018).
37. D. Breitling et al., "Material-vapor dynamics during ablation with ultrashort pulses," *Proc. SPIE* **5063**, 81 (2003).
38. S. M. Klimentov et al., "Effect of nonlinear scattering of radiation in air on material ablation by femtosecond laser pulses," *Proc. SPIE* **5121**, 77 (2002).
39. S. Klimentov et al., "Spectral dependences of conical emission in gases: Minimization of scattering for ultra-short pulsed laser ablation," *Laser Phys.* **19**(6), 1282–1287 (2009).
40. S. Klimentov et al., "Conical emission in focused beams: analysis of contributing factors and elimination of scattering," *Appl. Phys. B* **105**(3), 495–501 (2011).
41. V. P. Zhukov and N. M. Bulgakova, "Role of ambient gas in heating of metal samples by femtosecond pulses of laser radiation," *Thermophys. Aeromech.* **16**(2), 165–176 (2009).
42. N. Bulgakova et al., "Impacts of ambient and ablation plasmas on short- and ultrashort-pulse laser processing of surfaces," *Micromachines* **5**(4), 1344–1372 (2014).
43. D. Breitling, A. Ruf, and F. Dausinger, "Fundamental aspects in machining of metals with short and ultrashort laser pulses," *Proc. SPIE* **5339**, 49–63 (2004).

44. C. Foehl et al., "Precision drilling of metals and ceramics with short- and ultrashort-pulsed solid state lasers," *Proc. SPIE* **4426**, 104–107 (2001).
45. T. Abeln et al., "Helical cutting of holes in workpieces, involves rotating pulsed laser beam plane of polarization during beam movement so it is always at same angle to linearly machined cut surface," DE10105346A1, Germany (2001).
46. K. Jasper, *Neue Konzepte der Laserstrahlformung und -führung für die Mikrotechnik*, Utz Verl. Wissenschaft, München (2003).
47. C. Föhl, *Einsatz ultrakurz gepulster Laserstrahlung zum Präzisionsbohren von Metallen*, Utz Wiss, München (2011).
48. A. E. Siegman, *Lasers*, University Science Books, Mill Valley, California (1986).
49. M. A. Pate, "Optical design and specification of telecentric optical systems," *Proc. SPIE* **3482**, 877 (1998).
50. C. Foehl and F. Dausinger, "High precision deep drilling with ultrashort pulses," *Proc. SPIE* **5063**, 346–351 (2003).
51. M. Abramowitz and I. A. Stegun, eds., Handbook of Mathematical Functions, Dover Publisher, New York, NY (1972).
52. Pulsar Photonics GmbH, "MultiBeam scanner MBS G3," https://www.pulsar-photonics.de/en/system-technology/multibeam-scanner-mbs/ (accessed 26 August 2019).
53. O. Hofmann et al., "Highly dynamic positioning of individual laser beams in a multi-beam system for laser surface processing," *Proc. CIRP* **94**, 812–816 (2020).
54. J. Finger and M. Hesker, "High power ultrashort pulse laser processing using a flexible multibeam approach," *J. Phys. Photonics* **3**(2), 21004 (2021).
55. T. Barthels and M. Reininghaus, "High precision ultrashort pulsed laser drilling of thin metal foils by means of multibeam processing," *Proc. SPIE* **10744**, 107440B (2018).
56. Pulsar Photonics GmbH, "Flexible beam shaper FBS G3," https://www.pulsar-photonics.de/en/system-technology/flexible-beam-shaper/ (accessed 26 August 2019).
57. A. Meyer and M. Zuric, "Multi-beam processing with individually addressable beamlets: calibration & data processing," *JLMN* **16**(2), 100–108 (2021).

David Brinkmeier is working as a research associate and is PhD candidate at the IFSW (Institut für Strahlwerkzeuge) of the University of Stuttgart, Germany. His research interests include system technology for laser-based manufacturing and ultrafast laser processing of materials.

Volkher Onuseit received his diploma in mechanical engineering at the University of Stuttgart. From 2012 to 2015, he was working as head of the precision manufacturing group in the material processing department of IFSW, and since 2015, he has been in charge of the department for system engineering at IFSW.

Thomas Graf is working as professor at the University of Stuttgart and head of the IFSW.